J|A|C|S
ARTICLES
Published on Web 05/13/2003

Towards Graphite: Magnetic Properties of Large Polybenzenoid Hydrocarbons†

Damian Moran,‡,§ Frank Stahl,‡,§ Holger F. Bettinger,|| Henry F. Schaefer III,§ and Paul v. R. Schleyer*,‡,§

Contribution from the Institut für Organische Chemie, Friedrich-Alexander-Universität Erlangen-Nürnberg, Nägelsbachstr. 25, 91054 Erlangen, Germany, Center for Computational Quantum Chemistry, University of Georgia, 1004 Cedar Street, Athens, Georgia 30602-2525, and Institut für Organische Chemie II, Ruhr Universität Bochum, Universitätsstr. 150, 44780 Bochum, Germany

Received February 4, 2003; E-mail: schleyer@chem.uga.edu

Abstract: The geometries of four different series of D_{6h}-symmetric polybenzenoid hydrocarbons (PBH) up to and including $C_{222}H_{42}$ have been optimized at the B3LYP/6-31G(d) level of theory. Excluding $C_{48}H_{24}$ and $C_{138}H_{42}$, which have D_{3d} minima due to 1,5 H···H repulsions between adjacent perimeter rings, optimized geometries are planar D_{6h} minima. Nucleus Independent Chemical Shifts (NICS), at the same level, indicate the presence of individual aromatic rings, which correspond to Clar's qualitative sextets rule (Clar, E. *The Aromatic Sextet*; Wiley: London, 1972). NICS and the Clar valence electron topologies agree perfectly in the molecule plane; however, the NICS values computed in parallel planes further away from the molecular surface converge, indicating the presence of a uniform magnetic shielding field. For each series, PBH total NICS values (i.e., the sum of NICS values for all rings in the PBH) correlate linearly with the number of carbon atoms, indicating constant magnetic field development within a series. The C−C lengths depend on their proximity to the more olefinic rich molecular perimeters. However, the large PBH ($\geq C_{48}H_{24}$) internal C−C distances converge to ~1.426 Å. In agreement with Clar's rule, HF/6-31G(d)//B3LYP/6-31G(d) vertical ionization potentials and B3LYP/6-31G(d) HOMO−LUMO gaps are largest within the "fully benzenoid" series, where all carbon atoms are members of a single sextet. The largest members of the four series studied are predicted to exhibit semiconducting properties.

Introduction

If benzene (**1**) is the prototypical aromatic, then graphite is its ultimate expression. Graphite, the most stable form of carbon, is more aromatic than benzene, i.e., the resonance energy per pi electron (REPE) is greater. This leads to the question, how many six-membered rings elaborating benzene are needed to confer graphite-like properties? The first example with D_{6h}-symmetry is coronene (**2**), believed to be a "super-aromatic"[1] with a higher REPE than benzene (0.14 eV).[2]

Moreover, **2** does not follow the Hückel $4n+2$ rule. Although this applies strictly to regular monocyclic rings, it is often extended to polyaromatic hydrocarbons such as naphthalene and its higher homologues. Attention has been called to the [18]-annulene outer and the [6]annulene inner "perimeters" of coronene as a possible way to reconcile its lack of compliance with the $4n+2$ rule. However, this is not consistent with the NICS values (central ring: −5.3 ppm; outer rings: −12.9 ppm)[3] and related magnetic behavior,[4] which indicates a markedly reduced ring current in the central ring.

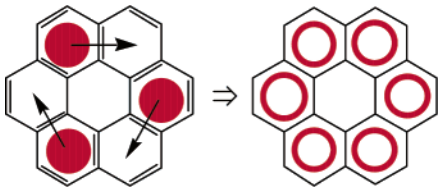

Figure 1. Coronene (**2**) Kekulé structure, with arrows included to indicate Clar sextet migration and their superposition that results in the NICS aromaticity pattern shown in Figure 3.

An alternative interpretation is provided by the formalism developed by Clar in his extensive studies of polybenzenoid hydrocarbons (PBH).[5−7] Clar assigns electron sextets, indicated by solid red circles in the figures (e.g., Figure 1) to discrete rings in PBH's and the remaining electrons to double bonds. Note that electrons can only be arranged in pairs, as Clar's

† Presented in part at the 2002 meeting of the World Association of Theoretically Oriented Chemists (WATOC) in Lugano, Switzerland.

‡ Institut für Organische Chemie, Friedrich-Alexander-Universität Erlangen-Nürnberg.

§ Center for Computational Quantum Chemistry, University of Georgia.

|| Institut für Organische Chemie II, Ruhr Universität Bochum.

(1) Clar, E.; Sanigök, Ü.; Zander, M. *Tetrahedron* **1968**, *24*, 2817.
(2) Randic, M.; Guo, X. F. *New J. Chem.* **1999**, *23*, 251.
(3) Buhl, M. *Chem. Eur. J.* **1998**, *4*, 734.
(4) Steiner, E.; Fowler, P. W.; Jenneskens, L. W. *Angew. Chem., Int. Ed. Engl.* **2001**, *40*, 362.
(5) Clar, E. *Polycyclic Hydrocarbons*; Academic Press Inc.: London, 1964; Vol. 1.
(6) Clar, E. *Polycyclic Hydrocarbons*; Academic Press Inc.: London, 1964; Vol. 2.
(7) Clar, E. *The Aromatic Sextet*; Wiley: London, 1972.

10.1021/ja034497z CCC: $25.00

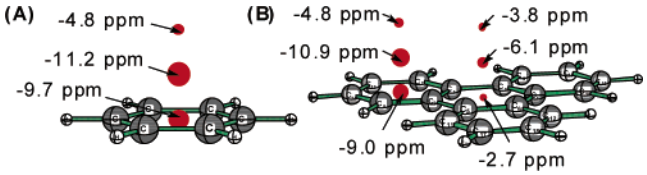

Figure 2. Benzene (A) and triphenylene (B) NICS values (ppm) 0, 1, and 2 Å above the ring plane(s). NICS 1 Å is used to assess PBH aromaticity patterns because π-electron ring current effects are dominant and local σ bonding contributions are diminished.

rule[5−7] forbids biradical character. Molecules with 6n π electrons and a single Kekulé structure that has all carbon atoms in sextet rings are so-called "fully benzenoid". On this basis, coronene is not fully benzenoid as it can only have three sextet rings at most; not only the central, but also three of the outer rings do not qualify. However, Clar proposed that "if the three sextets in coronene migrate into the neighboring rings a further ring current, originating from the rotating sextets, must be formed as indicated by the arrows" in Figure 1. Coronene's superaromaticity, Clar rationalized,[7] was due to contributions from its local sextet ring currents and the molecular sextet migration current.

Apart from the trivial example of benzene, triphenylene (Figure 2) is the smallest possible fully benzenoid PBH because all carbons are in sextet rings. Although triphenylene has three isolated sextets, it is not possible to assign more than two sextets to its *cata*-condensed $C_{18}H_{12}$ isomers such as benz[*a*]anthracene, chrysene, [4]helicene and naphthacene. Notably, among the $C_{18}H_{12}$ isomers, triphenylene has the largest resonance energy, is chemically least reactive, has the highest first ionization potential (IP), and has the largest HOMO−LUMO gap.[8] Computed PBH stabilities are often assessed using these latter two criteria. For example, Stein and Brown[9−11] used HOMO−LUMO gaps from Hückel MO theory[12] to compute the stabilities of four different series of D_{6h} polybenzenoid systems (the first few members of which are shown in Figure 3). Their key finding was the dramatic effect of the different perimeter structures on PBH stability; with Series 2 and 3 most stable, followed by Series 4 and then Series 1.[10,11] These findings have been rationalized by mean-field resonance theory[13−15] and conjugated-circuits theory.[16−19]

The present paper explores the geometries, magnetic properties, ionization potentials (IP) and HOMO−LUMO gaps of the first few members of Stein and Brown's[9−11] four different *peri*-condensed PBH series systematically using hybrid HF/DFT (B3LYP) and the 6-31G(d) basis set. Each series (series 1: **2**−**6**; series 2: **7**−**10**; series 3: **11**; and series 4: **12**−**13**) begins with benzene and expands by developing different edge and corner structures (see Figure 3; note that **7** and **9** are members of both series 2 and 3).[20]

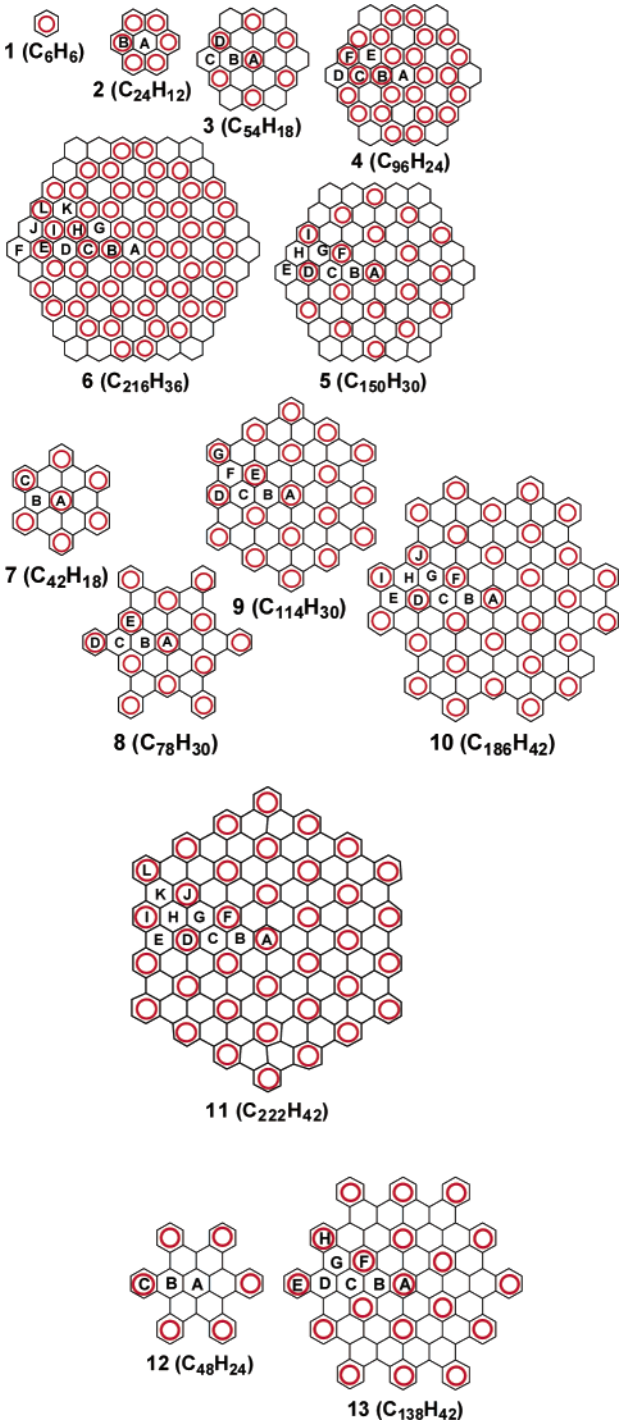

Figure 3. PBH aromatic rings (indicated by red circles) according to NICS in D_{6h} symmetric Series 1 (**2**−**6**), 2 (**7**−**10**), 3 (**11**), and D_{3d} symmetric Series 4 (**12**−**13**) structures. Upper case letters label inequivalent rings.

We seek answers to a number of questions. If graphite is the ultimate expression of prototypal aromatic benzene, then what are the properties of intermediate sized PBH? That is, when do C−C bond lengths equalize and graphite-like structural homogeneities develop? When do PBH magnetic fields become uniform? What is the effect of the PBH edge structures? Do the large PBH's have small HOMO−LUMO band gaps and semiconductor properties? Our results, which support earlier observations regarding edge structure effects on PBH geometries (vide infra), highlight the size independence of PBH magnetic properties and reveal that NICS is a robust and efficient tool

(8) Zander, M. *Polycyclische Aromaten-Kohlenwasserstoff und Fullerene*; Teubner: Stuttgart, 1995.
(9) Stein, S. E.; Brown, R. L. *Carbon* **1985**, *23*, 105.
(10) Stein, S. E.; Brown, R. L. In *Molecular Structure and Energetics*; Liebman, J. F., Greenberg, A., Eds.; VCH: Weinheim, 1987; Vol. 2, pp 37−66.
(11) Stein, S. E.; Brown, R. L. *J. Am. Chem. Soc.* **1987**, *109*, 3721.
(12) Heilbronner, E.; Bock, H. *The HMO Model and its Application*; Wiley-Interscience: New York, 1976.
(13) Ivanciuc, O.; Bytautas, L.; Klein, D. J. *J. Chem. Phys.* **2002**, *116*, 4735.
(14) Ivanciuc, O.; Klein, D. J.; Bytautas, L. *Carbon* **2002**, *40*, 2063.
(15) Klein, D. J.; Bytautas, L. *J. Phys. Chem. A* **1999**, *103*, 5196.
(16) Herndon, W. C. *J. Am. Chem. Soc.* **1990**, *112*, 4546.
(17) Herndon, W. C. *J. Am. Chem. Soc.* **1973**, *95*, 2404.
(18) Randic, M. *J. Am. Chem. Soc.* **1977**, *99*, 444.
(19) Randic, M. *Tetrahedron* **1977**, *33*, 1905.

for rapidly identifying and rationalizing Clar sextet electron localization patterns. Coulson[21] pointed out as early as 1954 that large PBH's (so-called graphenes) would be related to graphite structurally; we now propose that they have similar utility as 2-D graphite magnetic models.

Methods

The geometries of the polybenzenoid hydrocarbon structures shown in Figure 3 were optimized (B3LYP/6-31G(d)) in D_{6h} symmetry.[22] Vibrational frequencies (at the same level) were computed for **2**, **3**, **7**, **8**, and **12**. Series 4 structures (**12** and **13**) also were optimized at B3LYP/6-31G(d) in D_{3d} symmetry. Frequencies were computed at B3LYP/6-31G(d)//B3LYP/6-31G(d) for **12** and B3LYP/3-21G//B3LYP/3-21G for **13**. The B3LYP/6-31G(d) wave functions of **2**, **3**, **7**, and **12** (D_{6h} and D_{3d}) were stable.

Following our recommendations and earlier practice,[23,24] B3LYP/6-31G(d) NICS values were computed (GIAO approach) at ring centers, or as grids of points above optimized PBH surfaces where local contributions become less important. The NICS values for the largest PBH **11** were computed similarly, but using the 6-31G basis set (i.e., B3LYP/6-31G//B3LYP/6-31G(d)).

Vertical IP's (i.e., Koopmans[25] IP) for all members of the four PBH Series are given by the HF/6-31G(d) eigenvalue of the HOMO. For the smaller systems, B3LYP/6-31G(d) vertical IP's were computed using the cation energy at the neutral geometry. Both Hartree−Fock and Density Functional Theory are known to reproduce experimental ionization potentials with reasonable accuracy.[22,26−28] Koopmans IP's also were computed using the B3LYP/6-31G(d) HOMO eigenvalues; however, these were, as expected, consistently smaller than the experimental and HF values.[27,28]

Optimized geometries, vibrational frequencies and NICS were computed using the Gaussian 98 program package.[29] Harmonic Oscillator Model of Aromaticity (HOMA)[30−32] indices were derived by using the CHOMA program.[33] Optimized bond lengths, frequencies and NICS are included in the Supporting Information.

Table 1. NICS values (ppm) at 1 Å above PBH Molecular Planes (cf. benzene NICS (1 Å) = −11.2 ppm)

ring	2	3	4	5	6	7	8
A	−5.3	−16.2	−7.2	−15.5	−8.6	−15.1	−15.3
B	−12.9	−8.8	−14.6	−9.5	−15.1	−3.2	−5.5
C		−9.2	−14.5	−10.0	−14.9	−11.5	−4.6
D		−17.5	−4.4	−17.7	−8.4		−10.4
E			−7.0	−0.4	−18.9		−14.4
F			−16.8	−16.0	+2.6		
G				−9.5	−8.4		
H				−12.2	−15.7		
I				−18.7	−14.5		
J					−7.3		
K					−8.1		
L					−18.0		

ring	9	10	11	12	12 (D_{3d})[a]	13	13 (D_{3d})[a]
A	−16.1	−16.3	−15.4	+0.8	+0.1	−15.5	−15.5
B	−4.8	−6.0	−5.0	−7.5	−7.1	−3.5	−4.2
C	−2.4	−5.3	−3.9	−11.4	−9.2	−1.4	+0.3
D	−12.4	−16.0	−14.1			−8.0	−7.5
E	−14.9	−0.3	−4.2			−11.6	−8.5
F	−3.1	−15.9	−14.9			−12.8	−13.5
G	−12.5	−4.1	−3.9			−4.2	−4.3
H		−1.8	−0.9			−12.6	−12.3
I		−11.6	−12.2				
J		−14.3	−13.9				
K			−2.3				
L			−11.7				

[a] D_{3d} PBH surfaces are nonsymmetry equivalent and the average NICS per ring is reported.

Results and Discussion

Magnetic Properties. An external magnetic field induces local as well as delocalized magnetic fields in closed shell species;[24,34] the latter distinguish aromatic and antiaromatic species by diatropic and paratropic ring currents, respectively.[35] Hence, in an external magnetic field, aromatic and antiaromatic ring centers are shielded and deshielded, respectively. Schleyer et al.[23,24,36] introduced NICS as a criterion for aromaticity, whereby shieldings are computed directly and their signs simply reversed to comply with the "chemical shift" convention. Their magnitude is then assessed relative to the archetype aromatic **1**, which has NICS values of −9.6 (0 Å), −11.2 (1 Å), and −4.7 (2 Å), respectively (see Figure 2).

PBH NICS values are tabulated in Table 1 and summarized graphically in Figure 3, where aromatic rings are indicated using red circles. Relative to benzene, the individual rings in Series 2 and 3 structures are exclusively aromatic (NICS ≥ −10 ppm) or nonaromatic, and the distribution of aromatic centers in **7**-**11** is in perfect agreement with Clar's isolated sextet rule. In contrast, Series 1 and 4 PBH are more difficult to summarize because they include structures with moderately diatropic rings (e.g., rings D (−7.5 ppm) and E (−8.5 ppm) in D_{3d} **13**) and/or adjacent aromatic rings (e.g., rings B (−14.6 ppm) and C (−14.5 ppm) in **4**). The picture is further complicated in structure **5**, where all rings but E (−0.4 ppm) are significantly diatropic

(20) Müllen and co-workers recently prepared a number of large ($\geq C_{222}$) PAHs (Simpson, C. D.; Brand, J. D.; Berresheim, A. J.; Przybilla, L.; Räder, H. J.; Müllen, K. *Chem. Eur. J.* **2002**, *8*, 1424; Watson, M. D.; Fechtenkötter, A.; Müllen, K. *Chem. Rev.* **2001**, *101*, 1267; Schmidt-Mende, L.; Fechtenkötter, A.; Müllen, K.; Moons, E.; Friend, R. H.; MacKenzie, J. D. *Science* **2001**, *293*, 1119; Becker, S.; Müllen, K. In *Stimulating Concepts in Chemistry*; Stoddart, F., Shibasaki, M., Vögtle, F., Eds.; WILEY VCH: **2000**, pp 317−337; Dötz, F.; Brand, J. D.; Ito, S.; Gherghel, L.; Müllen, K. *J. Am. Chem Soc.* **2000**, *122*, 7707; Weiss, K.; Beernink, G.; Dötz, F.; Birkner, A.; Müllen, K.; Woll, C. H. *Angew. Chem., Int. Ed. Engl.* **1999**, *38*, 3748; Iyer, V. I.; Yoshimura, K.; Enkelmann, V.; Epsch, R.; Rabe, J. P.; Müllen, K. *Angew. Chem., Int. Ed. Engl.* **1998**, *37*, 2696; and references therein) using their newly developed synthetic approach.
(21) Coulson, C. A. *J. Chem. Soc.* **1954**, 3111.
(22) Hehre, W. J.; Radom, L.; Pople, J. A.; Schleyer, P. v. R. *Ab Initio Molecular Orbital Theory*; John Wiley & Sons: New York, 1986.
(23) Schleyer, P. v. R.; Jiao, H.; Hommes, N. J. R. v. E.; Malkin, V. G.; Malkina, O. L. *J. Am. Chem. Soc.* **1997**, *119*, 12 669.
(24) Schleyer, P. v. R.; Manoharan, M.; Wang, Z.-X.; Kiran, B.; Jiao, H.; Puchta, R.; Hommes, N. J. R. v. E. *Org. Lett.* **2001**, *3*, 2465.
(25) Koopmans, T. *Physica* **1934**, *1*, 104.
(26) Szabo, A.; Ostlund, N. S. *Modern Quantum Chemistry*; Macmillan: New York, 1982.
(27) Koch, W.; Holthausen, M. C. *A Chemist's Guide to Density Functional Theory*; Wiley-VCH: Weinheim, 2000.
(28) Curtiss, L. A.; Redfern, P. C.; Raghavachari, K.; Pople, J. A. *J. Chem. Phys.* **1998**, *109*, 42.
(29) Frisch, M. J.; Trucks, G. W.; Schlegel, H. B.; Scuseria, G. E.; Robb, M. A.; Cheeseman, J. R.; Zakrzewski, V. G.; Montgomery, J. A.; Stratmann, R. E.; Burant, J. C.; Dapprich, S.; Millam, J. M.; Daniels, A. D.; Kudin, K. N.; Strain, M. C.; Farkas, O.; Tomasi, J.; Barone, V.; Cossi, M.; Cammi, R.; Mennucci, B.; Pomelli, C.; Adamo, C.; Clifford, S.; Ochterski, J.; Petersson, G. A.; Ayala, P. Y.; Cui, Q.; Morokuma, K.; Malick, D. K.; Rabuck, A. D.; Raghavachari, K.; Foresman, J. B.; Cioslowsk, J.; Ortiz, J. V.; Stefanov, B. B.; Liu, G.; Liashenko, A.; Piskorz, P.; Komaromi, I.; Gomperts, R.; Martin, R. L.; Fox, D. J.; Keith, T.; Al-Laham, M. A.; Peng, C. Y.; Nanayakkara, A.; Gonzalez, C.; Challacombe, M.; Gill, P. M. W.; Johnson, B. G.; Chen, W.; Wong, M. W.; Andres, J. L.; Head-Gordon, M.; Replogle, E. S.; Pople, J. A.; *Gaussian 98*; revision A.5; Gaussian, Inc.: Pittsburgh, PA, 1998.
(30) Cyranski, M. K.; Krygowski, T. M.; Katritzky, A. R.; Schleyer, P. v. R. *J. Org. Chem.* **2002**, *67*, 1333.
(31) Krygowski, T. M.; Cyranski, M. K. *Tetrahedron* **1996**, *52*, 1713.
(32) Cyranski, M. K.; Krygowski, T. M. *J. Chem. Inf. Comput. Sci.* **1996**, *36*, 1142.
(33) Horn, A. H. C.: Erlangen, 2002.
(34) Moran, D.; Manoharan, M.; Heine, T.; Schleyer, P. v. R. *Org. Lett.* **2003**, *5*, 23.
(35) Pauling, L. *J. Phys. Chem.* **1936**, *4*, 673.
(36) Schleyer, P. v. R.; Maerker, C.; Dransfeld, A.; Jiao, H. J.; Hommes, N. J. r. V. E. *J. Am. Chem. Soc.* **1996**, *118*, 6317.

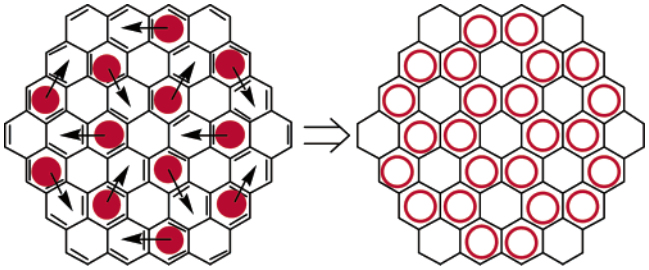

Figure 4. $C_{96}H_{24}$ (**4**) Kekulé structure (left); the arrows show Clar sextet (solid red dot) migration, which is responsible for the NICS aromaticity pattern on the right.

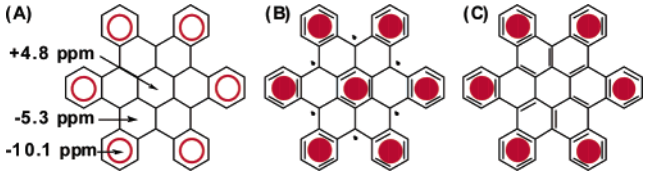

Figure 5. $C_{48}H_{24}$ (A) NICS, (B) hexaradical forbidden Clar formula and (C) fully benzenoid Clar formula.

(NICS ≥ −9.5 ppm). The resolution to these problems is found using a structure by structure analysis. For example, only those rings in structures **3** and **5** distinguished by NICS values ≥ −15.5 ppm are concluded to be aromatic because they are significantly more diatropic than the remaining rings in these molecules.

The adjacent aromatic rings found in structures **2**, **4**, and **6** are unavoidable, as an isolated aromatic ring pattern would require a D_{3h} symmetric wave function and the NICS patterns shown in Figure 3 are simply a consequence of the D_{6h} molecular symmetry. The effect of symmetry is demonstrated in Figures 1 and 4, which show that the NICS configurations for **2** and **4**, respectively, are the products of Kekulé structure superposition. Clar's rule forbids adjacent aromatic rings and uses arrows indicating "sextet migration" to account for the presence of degenerate (in this case D_{3h}) Clar structures.

The D_{6h} **6** (+2.6 ppm), D_{3d} **12** (+0.1 ppm), and D_{3d} **13** (+0.3 ppm) PBH's have positive (i.e., weakly paratropic) NICS, caused by the combination of π-electron localizing exocyclic C−C double bonds[37] and shielding σ-framework influences.[34,36] The [6]-radialene structure of **12** shown in Figure 5C, where the central antiaromatic ring is necessary to prevent the formation of a Clar forbidden hexaradical, is more remarkable. The central ring (1.441 Å) and radialene "spoke" (1.405 Å) optimized bond lengths agree. The approximately equal diatropicities of rings D and E in D_{3d} **13** is an artifact, and the problem is resolved by comparison with the D_{6h} **13** NICS values. Overall, the **12** and **13** D_{3d} NICS values are diminished relative to their D_{6h} counterparts, reflecting the decreased separation of σ and π shielding contributions in the nonplanar structures.

Clearly differentiated Clar sextet ring patterns occur in the molecular planes of D_{6h} PBH's. However, above molecular planes, uniform magnetic fields develop and graphite-like properties appear, although graphite-like PBH dimensions have not been approached. Figure 6 shows that NICS values, placed above the PBH surface, tend to a uniform value for even the relatively small PBH **7**. In the molecular plane, the deviation between A (−13.5 ppm), B (+0.9 ppm) and C (−9.5 ppm) ring

(37) Schleyer, P. v. R.; Puhlhofer, F. *Org. Lett.* **2002**, *4*, 2873.

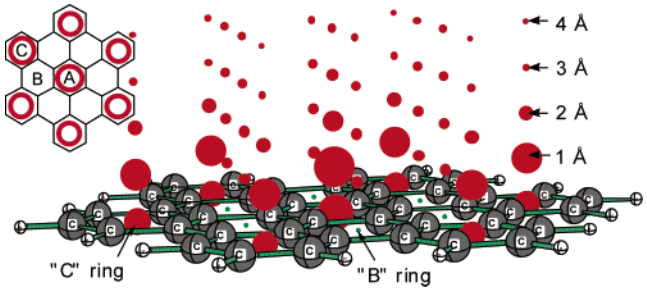

Figure 6. $C_{42}H_{18}$ NICS grid. Extending to 4 Å, the grid shows the trend toward a uniform magnetic field (i.e., NICS points develop uniform size) above PBH ring planes.

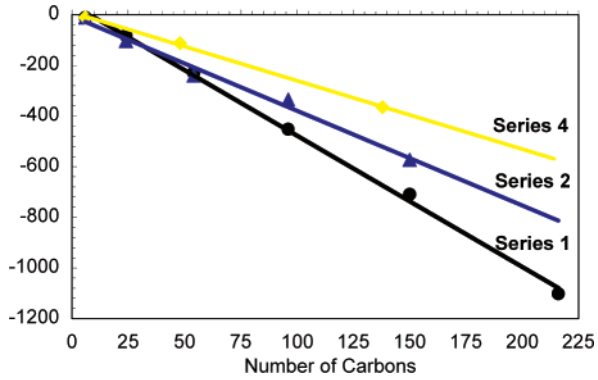

Figure 7. Combined PBH 1 Å NICS (ppm) plotted against the number of PBH carbons (which also is the total number of π-electrons). Lines of best fit connect members from related series.

NICS is > 10 ppm. However, at 2 Å above the PBH the A (−7.3 ppm), B (−3.4 ppm), and C (−5.0 ppm) the ring NICS values are much closer in magnitude and at 4 Å they approach uniformity (A: −2.6 ppm; B: −2.1 ppm; C: −1.5 ppm).

The summation of NICS values for a given PBH sheet leads to a single quantity called the "total NICS". Plotted against the number of PBH carbons (Figure 7), which coincidentally also is the number of π electrons, total NICS values differentiate PBH into their respective series. The remarkable ability of NICS to separate the different PBH series is quantitative, with lines of best fit correlating total NICS and PBH series almost prefectly ($R \geq 0.99$).

Comparison of HF/6-31G(d), which neglects electron correlation, and B3LYP/6-31G(d) optimized PBH geometries (see figures in the Supporting Information) reveals small, but ubiquitous differences between bond lengths predicted using the HF and hybrid HF-DFT theories (vide infra). In contrast, PBH NICS values show suprisingly good agreement irrespective of the level of theory or the geometry (i.e., HF and HF-DFT optimized) employed. For example, Table S1 (Supporting Information) HF/3-21G//HF/6-31G(d), HF/6-31G(d)//HF/6-31G(d) and B3LYP/6-31G(d)//B3LYP/6-31G(d) GIAO ring center NICS are almost identical.

Geometries. With the exception of **12** and **13** (series 4 structures), all PBH's for which frequencies were computed have D_{6h} minima.[38] Mode following the planar Series 4 structures primary imaginary vibrational frequencies led to the D_{3d} minima shown in Figure 8. Unfavorable 1,5-bumping between perimeter hydrogens destabilizes the planar Series 4 structures and the D_{3d} minima are 162 (**12**) and 348 (**13**) kcal/mol lower in energy. This situation anticipates the greater repulsive interactions in helicenes, which preclude planar geometries.[39]

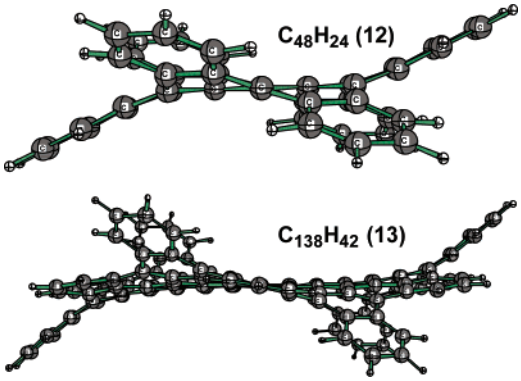

Figure 8. Optimized D_{3d} Series 4 structures; they are 162 ($C_{48}H_{24}$) and 348 ($C_{138}H_{42}$) kcal/mol more stable than their respective planar D_{6h} isomers.

The average (vide infra) B3LYP/6-31G(d) optimized Series 1, 2, 3, and 4 PBH C−C distances are 1.425, 1.429, 1.427, and 1.426 Å, respectively. Comparisons with Negri et al's[40] BLYP/6-31G optimized PBH bond lengths, which range between 1.43 and 1.45 Å reveals pleasing agreement between our hybrid HF/DFT and their pure DFT bond distances. In contrast, Weinert et al.[41] computed a bond length of 1.415 Å for an infinite 2-D graphite sheet using Born-Karman (periodic boundary) conditions and an all-electron plane-wave density functional theory ansatz. Additionally, Almlöf and Lüthi[42] reported a value of 1.406 Å for HF theory optimized (with equal C−C lengths imposed) **2**, **3**, and **4**, which is also shorter than the B3LYP/6-31G(d) optimized Series 1 average C−C distance.

Large PBH's are often considered to be models for an isolated graphite sheet. Graphite has a negative in-plane thermal expansion coefficient, i.e., the C−C bond length within each layer contracts and the interlayer distance increases upon heating.[43] Hence, an isolated graphite monolayer is expected to have a C−C bond length less than the distance (1.421 Å) in bulk graphite,[44] and closer to the benzene value of 1.391 Å.[45] However, these expectations are not met and the average B3LYP/6-31G(d) optimized C−C length, taken from all PBH, is ∼1.426 Å. The disparity, ∼0.005 Å, is due to the level of theory employed, as, for example, optimized benzene C−C lengths (HF/6-31G(d) = 1.386 Å; MP2/6-31G(d) = 1.395 Å; and B3LYP/6-31G(d) = 1.397 Å) vary somewhat with respect to the experimental value of 1.391 Å.[45] Hybrid HF/DFT theory overestimates the benzene bond length, as it does the PBH C−C distances when compared with expectations based on the graphite thermal expansion response.

As there are olefin-like short C−C bonds with lengths below 1.4 Å at the molecular perimeters, B3LYP/6-31G(d) optimized PBH geometries are strongly affected by the proportion of "edge structures" (see Figure 9). The internal C−C bond distances,

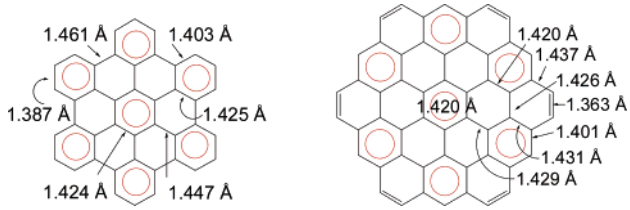

Figure 9. Small D_{6h} PBH's, e.g., $C_{42}H_{18}$ (left) and $C_{54}H_{18}$ (right) have significant bond length variations due to the large proportion of olefinic perimeter C−C bonds.

Table 2. Minimum (min), Maximum (max) and Average Internal (inter) and Total (internal + peripheral) Optimized Bond Lengths (Å), Including Standard Deviation (SD)[a]

PBH	min	max	inter	SD	min	max	total	SD
$C_{24}H_{12}$	1.421	1.428	1.425	0.005	1.372	1.428	1.411	0.026
$C_{42}H_{18}$	1.424	1.447	1.432	0.013	1.387	1.461	1.425	0.027
$C_{48}H_{24}$	1.431	1.492	1.455	0.033	1.370	1.492	1.432	0.046
D_{3d}	1.405	1.441	1.425	0.018	1.382	1.450	1.419	0.024
$C_{54}H_{18}$	1.420	1.431	1.425	0.005	1.363	1.437	1.416	0.024
$C_{78}H_{30}$	1.423	1.437	1.428	0.007	1.383	1.465	1.420	0.022
$C_{96}H_{24}$	1.417	1.438	1.425	0.006	1.359	1.443	1.418	0.021
$C_{114}H_{30}$	1.418	1.441	1.430	0.008	1.372	1.452	1.421	0.021
$C_{138}H_{42}$	1.425	1.473	1.443	0.014	1.353	1.483	1.431	0.035
D_{3d}	1.406	1.440	1.426	0.011	1.379	1.460	1.422	0.020
$C_{150}H_{30}$	1.415	1.443	1.425	0.007	1.357	1.446	1.418	0.022
$C_{186}H_{42}$	1.418	1.444	1.427	0.007	1.387	1.460	1.423	0.018
$C_{216}H_{36}$	1.410	1.446	1.425	0.008	1.356	1.446	1.420	0.017
$C_{222}H_{42}$	1.408	1.440	1.427	0.007	1.371	1.451	1.423	0.016

[a] Unless otherwise specified, geometries are D_{6h} symmetric.

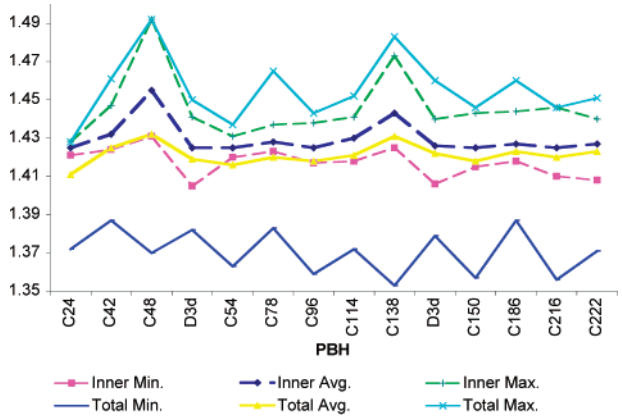

Figure 10. Minimum, average (dotted lines) and maximum internal and total (internal + peripheral) PBH bond length (Å). Unless indicated otherwise by a D_{3d} abscissa label, as shown for nonplanar $C_{48}H_{24}$ and $C_{138}H_{42}$, all PBH structures are D_{6h} symmetric. See Table 2 for absolute values.

for example, the **a**, **b**, and **c** bonds of **7** (see Figure S4 of the Supporting Information), have a much narrower range (1.41−1.44 Å). Therefore, to summarize the optimized PBH geometries, a distinction has been made between the "inner" and "total" (inner + perimeter) bond groups (see Table 2), with the former providing a better indication of trends in optimized bond lengths. The advantage of distinguishing between inner and total C−C bond lengths is indicated in Table 2, which is also graphically summarized in Figure 10. Note that Series 1 PBH have the same average inner C−C bond lengths (1.425 Å), indicating excellent bond length equalization within the series. With the exception of **7**, Series 2 average C−C lengths are also in good agreement with one another, although overall, they are slightly (+0.003) longer than in Series 1. Average Series 3 and 4 C−C distances fall between Series 1 and 2 carbon bond

(38) Samori, P.; Severin, N.; Simpson, C. D.; Müllen, K.; Rabe, J. P. *J. Am. Chem. Soc.* **2002**, *124*, 9454 report that molecular mechanics (PCFF) optimized $C_{42}H_{18}$ is distorted from planarity. However, a nonplanar starting geometry of **7**, optimized at B3LYP/6-31G(d) without any symmetry constraints, resulted in essential planarity.
(39) Lloyd, D. *The Chemistry of Conjugated Cyclic Compounds: To Be or Not To Be Like Benzene*?; John Wiley & Sons: Chichester, England, 1989.
(40) Negri, F.; Castiglioni, C.; Tommasini, M.; Zerbi, G. *J. Phys. Chem. A* **2002**, *106*, 3306.
(41) Weinert, M.; Wimmer, E.; Freeman, A. J. *Phys. Rev. B* **1982**, *26*, 4571.
(42) Almlöf, J.; Lüthi, H. P. In *ACS Symposium Series 353*; American Chemical Society: Washington, DC, 1987; pp 35−48.
(43) Ludsteck, A. *Acta Crystallogr. Sect. A* **1972**, *28*, 59.
(44) Donohue, J. D. *The Structure of the Elements*; Wiley-Interscience: New York, 1974.
(45) Gauss, J.; Stanton, J. F. *J. Phys. Chem. A* **2000**, *104*, 2865.

Table 3. Summary of PBH Koopmans Ionization Potentials (IP; eV) and HOMO−LUMO Gaps (H/L; eV), with Experimental and Literature Values Included Where Available

		IP			H/L		
series	PBH	exp[a]	HF[b]	DFT[c]	exp[d]	DFT	HF[e]
	1	9.25	9.0	6.7	6.2	6.8	
1	2	7.29	7.0	5.5	3.8	4.0	2.6
	3		6.1	4.9		2.8	1.9
	4		5.6	4.7		2.1	1.5
	5		5.2	4.5		1.6	1.3
	6		4.9	4.3		1.3	1.2
2	7	6.87	6.7	5.2	3.2	3.6	2.2
	8		6.2	5.0		2.9	-
	9		5.7	4.7		2.4	1.4
	10		5.4	4.6		2.0	-
3	11		5.2	4.5		1.8	1.0
4	12	6.75	7.0	5.4		3.5	2.2
	13		5.7	4.6		2.1	1.3

[a] Values taken from ref 46; the center of gravity of the set of signals within the p-band of the UV spectra was used. [b] HF/6-31G(d)//B3LYP/6-31G(d). [c] B3LYP/6-31G(d)//B3LYP/6-31G(d). [d] Values taken from refs 5−7. [e] Semiempirical extended HF theory (refs 48 and 49).

lengths. Using Hückel MO optimized PBH geometries, Stein and Brown[9−11] also noted the dramatic effect of the edge structure and reported equalization of bonds more than three or four rings away from the molecular perimeter.

Excluding **2**, Series 1−4 global HOMA[30−32] indicies (see Supporting Information) fall in the range 0.61−0.66. The global HOMA of the coronene X-ray geometry is 0.73,[32] which is higher than B3LYP/6-31G(d) optimized **2** (HOMA = 0.56) and reflects the difference between the predicted (A: 1.428 Å; B: 1.421 Å; C: 1.424 Å; D: 1.372 Å) and diffraction (A: 1.425 Å; B: 1.433 Å; C: 1.415 Å; D: 1.346 Å)[46] structures.

Ionization Potentials. PBH vertical IPs computed at the HF/6-31G(d) (i.e., Koopmans IPs) and B3LYP/6-31G(d) levels are summarized in Table 3. Both approaches agree and reproduce the available experimental values well. The Koopmans IPs are summarized graphically in Figure 11. Clar predicted enhanced stability for fully benzenoid systems and related this to large first ionization potentials.[7] Indeed, the curve for Series 1 PBH falls below the curve for the fully benzenoid Series 2 and 3, in agreement with Clar's predictions. Note that **7** and **9** are members of both Series 2 and 3,[9−11] hence they appear in both Series 2 and 3 curves. The D_{3d} symmetric Series 4 IP curve also is above the Series 1 PBH curve.

HOMO−LUMO Gaps. PAH UV-absorption spectra consist of the α, para, and β sets of bands, named in order of increasing intensity.[5−7] The para band corresponds to the HOMO−LUMO transition and the B3LYP/6-31G(d) HOMO−LUMO gaps summarized in Table 3 and Figure 11 mirror the available UV spectroscopic data[47] satisfactorily. The HOMO−LUMO gaps for **2**−**7**, **9**, **11**−**13** are consistently higher than those reported by Müllen and co-workers[48,49] based on semiempirical extended Hartree−Fock theory,[50] although the trends are qualitatively the same. Müllen and co-workers[48,49] found that extrapolation to infinitely large sheets yielded nonzero HOMO−LUMO gaps

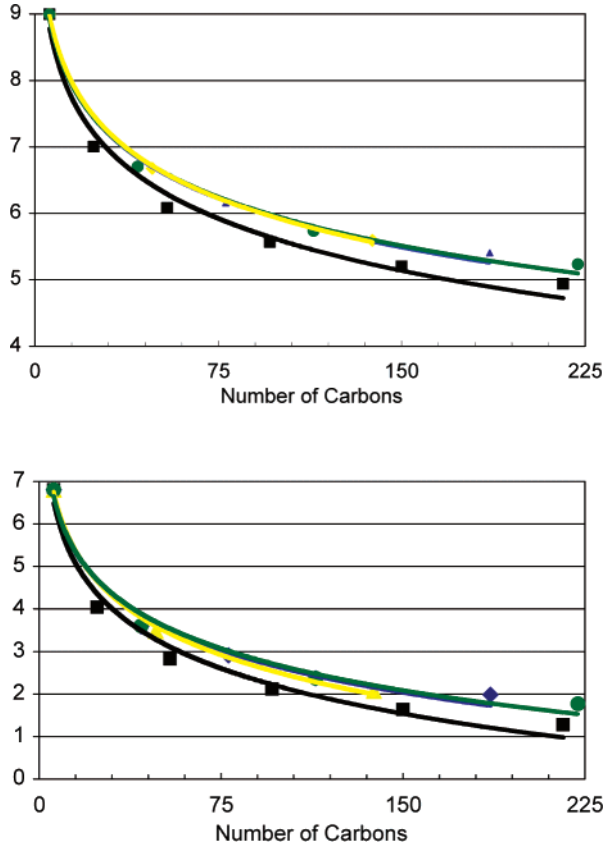

Figure 11. PBH Koopmans IPs (top; eV) and HOMO−LUMO gaps (bottom; eV) plotted against the total number of carbons. In both plots, the series 2, 3, and 4 lines of best fit overlap and are located above the Series 1 trend line. See Table 3 for absolute values.

and predicted, as did Almlöf and Lüthi,[42] that large PBH's are potential semiconductors. The HOMO−LUMO values in Table 3, although expected to be underestimated at HF and overestimated at B3LYP levels,[27] are related to the band gap of graphite.

The energy difference between the HOMO and the LUMO has been used as an index for kinetic stability.[51] Using this principle, Stein and Brown[9−11] reported that Series 2 and 3, followed by Series 4, were most stable, whereas Series 1 was most reactive. At the B3LYP/6-31G(d) level of theory the same stability order is predicted, i.e., series 2 > 3 > 4 > 1.

Conclusions

The geometries of four different series of peri-condensed D_{6h}-symmetric polybenzenoid hydrocarbons (PBH) with homologous edge and corner structures have been optimized at the B3LYP/6-31G(d) level of theory and the magnetic shieldings at individual ring centers (i.e., NICS) computed. Clar sextet rings have large negative NICS values in PBH, and overall there is perfect agreement between Clar and NICS π electron topologies. At 4 Å above PBH surfaces, NICS tend to equalize because an average magnetic field develops. PBH are related by their total NICS, which differentiates series 1, 2, 3, and 4 molecules into their respective structural groups. With the exception of the molecular perimeters, which are rich in short olefinic bonds, optimized bond lengths tend to equalize; average "internal" C−C ≈ 1.426 Å (cf. graphite C−C = 1.421 Å). Series 1 PBH's

(46) Fawcett, J. K.; Trotter, J. *Proc. R. Soc. Lon. Ser. A* **1966**, *289*, 366.
(47) Lias, S. G.; Bartmess, J. E.; Liebman, J. F.; Holmes, J. L.; Levin, R. D.; Mallam, W. G. *J. Phys. Chem. Ref. Data* **1988**, *17 (S1)*, 1.
(48) Tyutyulkov, N.; Madjarova, G.; Dietz, F.; Müllen, K. *J. Phys. Chem. B* **1998**, *102*, 10 183.
(49) Dietz, F.; Tyutyulkov, N.; Madjarova, G.; Müllen, K. *J. Phys. Chem. B* **2000**, *104*, 1746.
(50) Lowdin, P. O. *Phys. Rev.* **1955**, *97*, 1509.
(51) de Proft, F.; Geerlings, P. *Chem. Rev.* **2001**, *101*, 1451.

have the lowest IP's and the smallest HOMO−LUMO gaps and these structures are the least stable compared with series 2, 3, and 4 PBH.

In contrast with PBH geometries, which show ubiquitous differences when optimized using the HF versus hybrid HF-DFT theory, PBH NICS values are in excellent agreement irrespective of the level of theory or the geometry (i.e., HF and HF-DFT optimized) employed. The NICS "picture" of aromaticity, nonaromaticity and antiaromaticity predicted at B3LYP/6-31G(d) is also found at the much more economical HF/3-21G level of theory.

Acknowledgment. Dedicated to Ken Houk, in appreciation of his numerous contributions to computational chemistry, on the occasion of his 60th birthday. We are grateful to the University of Georgia, the Deutsche Forschungsgemeinschaft (DFG), the U. S. Department of Energy and the U. S. National Science Foundation (Grant No. CHE-0209857) for financial support. We thank Dr. Wesley Allen (University of Georgia), Dr. Doug Klein (Texas A&M University at Galveston), Dr. William Herndon (University of Texas at El Paso), Dr. Thomas Heine (Technische Universität Dresden, Germany), and Dr. Walter Thiel (Max-Planck-Institut für Kohlenforschung, Mülheim Germany) for fruitful discussions. H.F.B. thanks the Fonds der Chemischen Industrie for support through a Liebig fellowship and Dr. Wolfram Sander (Ruhr-Universität Bochum, Germany) for encouragement. D.M. thanks H. Lee Woodcock for his warm hospitality.

Supporting Information Available: Optimized bond lengths, NICS values, HOMA indicies, absolute energies, and harmonic vibrational frequencies are summarized in the Supporting Information. This material is available free of charge via the Internet at http://pubs.acs.org.

JA034497Z